CORA Cork Open Research Archive
Cartlann Taighde Oscailte Chorcaí

Title	Design of a foldable origami mechanism with helical motion inspired by the Resch Triangular Tessellation
Authors	Liang, Haitong;Hao, Guangbo;Olszewski, Oskar Z.;Jiang, Zhujin;Zhang, Ketao
Publication date	2022-10-02
Original Citation	Liang, H., Hao, G., Olszewski, O. Z., Jiang, Z. and Zhang, K. (2023) 'Design of a foldable origami mechanism with helical motion inspired by the Resch Triangular Tessellation', Mechanism and Machine Theory, 179, 105101 (17pp). https://doi.org/10.1016/j.mechmachtheory.2022.105101
Type of publication	Article (peer-reviewed)
Link to publisher's version	10.1016/j.mechmachtheory.2022.105101
Rights	© 2022, Elsevier B.V. All rights reserved. This manuscript version is made available under the CC BY-NC-ND 4.0 license. - https://creativecommons.org/licenses/by-nc-nd/4.0/
Download date	2026-11-06 03:49:56
Item downloaded from	https://hdl.handle.net/10468/16221

UCC
University College Cork, Ireland
Coláiste na hOllscoile Corcaigh

Design of a Foldable Origami Mechanism with Helical Motion Inspired by the Resch Triangular Tessellation*

Haitong Liang[1,2], Guangbo Hao[1,2*], Oskar Z. Olszewski[1], Zhujin Jiang[3], and Ketao Zhang[3]
[1] Tyndall National Institute, Lee Maltings Complex, Dyke Parade, Cork, Ireland, T12R5CP
[2] School of Engineering and Architecture, University College Cork, College Road, Cork, Ireland, T12K8AF
[3] Centre for Advanced Robotics (ARQ), Queen Mary University of London, Mile End Road, London E1 4NS, UK.
*Corresponding author: G.Hao@ucc.ie

Abstract: The central triangular panel of a minimum unit of the Resch Triangular Tessellation twists during the folding/unfolding process. Taking inspiration from this artistic origami, this paper presents a novel helical origami mechanism with a foldable/deployable form. It has 3-Degrees-of-Freedom (DoFs) and is capable of helical motion (one twisting motion coupled with the translation along with the same axis). The mechanism is extracted from an origami structure which consists of two minimum units of the Resch triangular tessellation pattern connecting in stack face to face. Three origami creases intersecting at a common point, equivalent to a traditional spherical joint, are adopted for the connection. The geometric and kinematic characteristics of the origami mechanism are analyzed. The workspace of the centre of the moving platform of the mechanism is analyzed. A proof-of-concept prototype of the mechanism is fabricated and experimentally demonstrated by a cable driven actuation system. The pure helical motion mode (when three inputs are the same) is tested using the prototype and is compared with the theoretical model. It is also demonstrated that the mechanism is able to change between folded and deployed configurations. Diverse motion configurations with different settings of input angles are presented by evaluating the 3D model and prototype of the novel helical mechanism. The connection of multiple helical origami mechanisms in series leads to a novel continuum robot which is also discussed. Compared with other multi-DOF counterparts, this novel origami mechanism is capable of the helical motion and diverse motion configurations corresponding to different actuation angles without flexible panels.
Keywords: Origami, Helical Motion, Resch Triangular Tessellation, Robot Mechanism.

1 Introduction

Origami is the art of folding a sheet of paper into various forms without stretching, cutting or gluing other pieces of paper to it [1, 2]. It was originally developed more for artistic purposes, folding sheets of paper into various shapes, either in abstract forms or mimicking certain objects [3]. Origami has attracted attention from various areas, such as architecture [4-6], mathematics [7-9], and engineering[10-12], because it enables complex 3D structures from folding a 2D material with crease patterns composed of all crease lines of the complex structure [13-15]. There are four basic crease patterns: the *Miura-ori pattern*, the *Waterbomb pattern*, the *Yoshimura pattern*, and the *Diagonal pattern* respectively. These crease patterns all belong to tessellation origami, where both the unfolded and folded states use repeated elements to form two-dimensional patterns [16, 17]. Resch Triangular Tessellation was developed by Ronald Resch in 1960s. It has repeated triangular patterns in both folded and unfolded states.

The origami concept is valuable in the field of robotics due to its transformation between 2D patterns and 3D structures through simple folding and unfolding. In addition, both mountain folds and valley folds can be seen as rotational joints from the aspect of robotics, which further highlights the

applicability of origami to robotics. There have been various types of origami-based robots reported in the literature and they are actuated in different methods [18-20]. Belke et al. published a robotic platform and reconfigurable modular robots based on origami theories [19]. Driven by micro stepper motors, different spatial configurations and functions could be achieved through folding motions among robotic modules. McClintock et al. reconstructed the Delta robot with origami techniques at millimeter-scale [21]. Actuated with three individual piezoelectric bending actuators, this milliDelta origami robot presented micrometer-level operation precision. Li et al. developed a light-weight, soft robotic gripper, which is composed of an origami structure based on a Waterbomb pattern and a flexible thin membrane [22]. Driven by vacuum, this origami gripper could lift a large variety of objects, showing great adaptability and robustness. Hao et al. proposed a deployable stent inspired by the bi-stable characteristics of a Waterbomb pattern [23]. Actuated and controlled by memory alloy wire, this design presented good bi-stability and deployability. Miyashita etc. developed a self-foldable origami device which could transform from a tiny sheet into a 3D functional structure under the remote control of alternating external magnetic field [20]. Nelson et al. presented origami-inspired sacrificial joints which can be obtained by folding steel sheets following pre-designed crease patterns [24]. Zhang et al. developed an origami parallel module which was composed of two triangular bases and three waterbomb bases [25, 26]. This mechanism can be seen as the classical 3-RSR mechanism realized in the novel origami form. Dai introduced the screw theory in the kinematic analysis of the origami-based mechanisms [27, 28] which prompted the development of this research area. Advantages shared by these origami-inspired robots include ultra-compact footprint, reduced weight, low cost, good manufacturability, free friction, etc.[29]

Helical motions from origami structures have been well studied in the literature [30, 31]. Jiang et al. developed an origami-inspired twisting skeleton which was actuated by an artificial muscle [31]. The desired helical motion was analytically and experimentally verified. Zhang et al. developed a segmented worm robot by successively integrating kirigami parallel structures with a helical motion [32]. Both peristalsis and inchworm-type motion in nature could be imitated with shape-memory-alloy linear actuators. Kresling proposed the Kresling patterns which were spontaneously generated from buckled cylindrical thin-wall shells under torsional load [33]. Origami mechanisms based on the Kresling patterns presented helical motions in their folding process [34, 35]. Berre et al. considered the Kresling tower origami with helical motion as a building component for the compliant mechanism design [36]. A model was derived in their research to describe the helical trajectory and bi-stable positions. Wu et al. introduced a magnetically controlled origami robotic arm based on Kresling patterns [35]. The origami robotic arm enabled multimodal motions, such as twisting, bending, and stretching. The Kresling origami patterns were also used in the design of reconfigurable helical antennas [37, 38]. The operating frequencies of the origami antennas could be adjusted by changing the height [38]. Hoff et al. adopted an origami twisted tower in a multimodal origami arm which was thread-actuated [39]. Jeong et al. used similar origami twisted components in their three-finger manipulator [40]. Yoneda et al. made a paper spring by folding and gluing together two thin strips of paper [41]. The helical motion of this paper spring was investigated theoretically and experimentally. The problem with the most helical origami mechanisms in literature is that the planes of the origami structures are not rigid [41, 42] and must deform in the folding process to produce the helical motions. It is because those origami designs are over-constrained and non-rigid foldable.

In this study, we aim to address the above issues/needs by proposing a new helical origami mechanism. This mechanism is inspired by Resch Triangular Tessellation is first proposed following the origami principles. It is constructed by connecting two minimum units face to face using the 3-hinged origami joints, which has 3 DoFs with rigid panels. The helical motion is the focus in this paper, which is

highly desired in many applications such as drilling a hole or achieving a rotation using a linear input [43]. If a pure helical motion is needed, a simple cylindrical constraint can be added to the end effector of the mechanism.

This paper is organized as follows. Section 2 provides a geometric analysis of the helical behaviour of the minimum unit of the Resch Triangular Tessellation. The primary design of the helical origami mechanism and its origami connecting joints are introduced in Section 3. In addition, the kinematic analysis of the helical origami mechanism is carried out and the workspace of the mechanism is analyzed in this section. A preliminary prototype of the origami mechanism is shown in Section 4 for the verification of the helical motion. Section 5 provides an expanded discussion on the diverse motion configurations of this helical origami mechanism with a 3D model and the prototype. This is followed by the introduction of an integrated origami robot composed of several helical origami mechanisms as modules in series. Conclusions and prospects are drawn in Section 6.

2 The Twisting Behavior of the Minimum Unit of Resch Triangular Tessellation

The Resch Triangular Tessellation (RTT), as shown in Fig. 1, is a typical example of origami tessellation design. It was patented by Ronald Resch, an artist, computer scientist and applied geometrist in the 1960s [44]. The crease pattern of this tessellation is composed of identical minimum units repeating in a certain order, which is illustrated in Fig. 1(a). During the transformation process from a 2D sheet gradually into a 3D structure (from the state in Fig. 1(a) to (e)), the triangular block in the center of each minimum unit twisted 30 degrees. This twisting behavior can be observed on every triangular minimum unit of Resch Triangular Tessellation. Each minimum unit is composed of four parts, one central plane and three identical external panels, as illustrated in Fig. 1(a). Since both the unit itself and the central plane are all triangular, their tip angles are all 60 degrees. The boundaries of the central plane are solid lines which are origami mountain folds. The central plane starts to twist when the three external panels are folded about the solid boundary (simultaneously at the same angular speed).

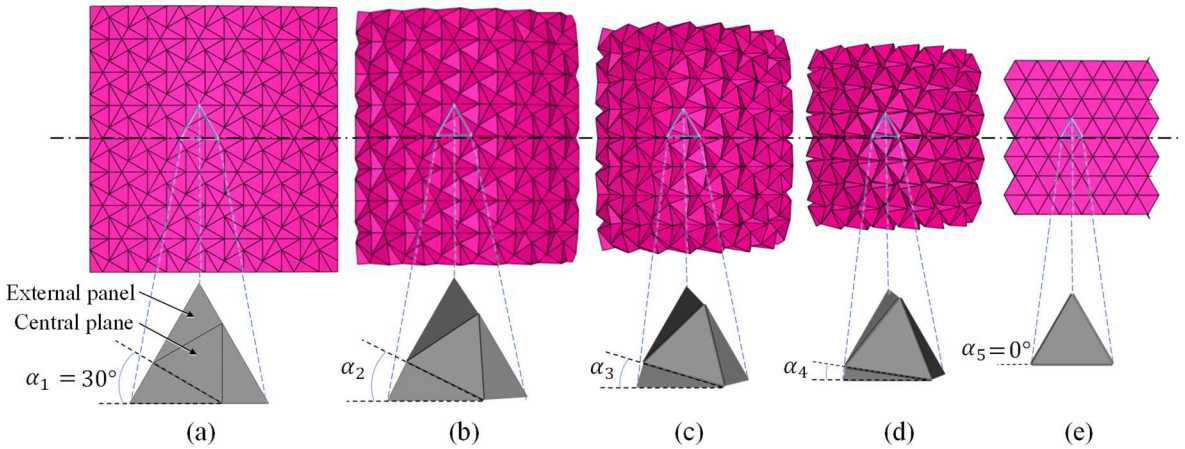


Fig. 1. The folding process of RTT and the twisting behaviour of the minimum unit [45].

The twisting behavior is further discussed based on the minimum unit as shown in Fig. 2. In the coordinate system o-xyz, a minimum unit is in a certain folding condition where external panels rotate with the identical angle of θ at an angular speed of ω. In x-y plane, the projective regular triangle ABC turns into A′B′C′ when the external planes rotate, while the central triangle plane is fixed in x-y plane.

α represents relative angle between the central triangle DEF and the changing projective triangle $A'B'C'$. α_C indicates the angular displacement of the triangle $A'B'C'$ relative to its initial position ABC, which is the twisting angle of the minimum unit. Height h represents the increase in the size of this unit in the z-direction. According to geometric knowledge, their relationship can be easily derived and described by the equations below:

$$\alpha = \arctan\left(\frac{2\cos\theta + 1}{\sqrt{3}}\right) - 30° \tag{1}$$

$$h = l \cdot \sin\theta \tag{2}$$

Rotational angle θ can be replaced by ωt, indicating the dynamic folding process. Therefore, the twisting angle of the central plane relative to the reference line, α_C, is:

$$\alpha_C = 60° - \arctan\left(\frac{2\cos\omega t + 1}{\sqrt{3}}\right) \tag{3}$$

According to the Eqs. (2) and (3), the twisting motion and the increase of the height in the z-direction are coupled with each other and are determined by the folding of three external panels. From this aspect, the minimum unit of Resch Triangular Tessellation behaves in a helical manner and its equivalent pitch is:

$$P = \frac{360°}{\alpha_{\mathrm{Cmax}}} \cdot l = 12l \tag{4}$$

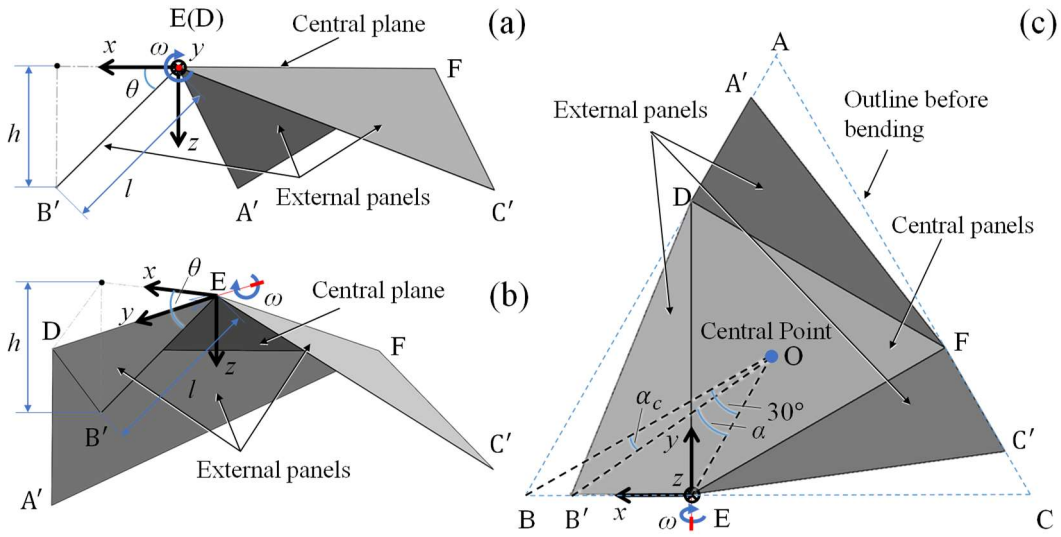


Fig. 2. Geometric parameters of the minimum unit of RTT in different views. (a) Side View; (b) Bottom-side view; (c) Top view.

3 Design and Modelling of the Helical Origami Mechanism

3.1 Kinematic Structure of the Helical Mechanism with a Spherical Joint

Inspired by the twisting behaviour of the RTT observed in its folding process, a helical origami mechanism is proposed and introduced in this section. The helical mechanism is designed primarily by arranging two identical minimum units (as shown in Fig. 2) face to face and connecting their three tip points, respectively. A spherical joint is employed in each limb to connect the upper and bottom units to conceive the helical motion. A 3D model of this helical mechanism is created with Solidworks® as shown in Fig. 3, where the spherical joints are indicated. In the 3D model, all panels are designed with an identical thickness of 2 mm. In real operations, the thickness of the panels is

expected to be thin but with sufficient strength to prevent deformation. It is selected based on both the geometries of the origami structures and the mechanical properties of the materials.

The expected helical motion is observed when the external panels of the bottom minimum unit fold up simultaneously with the identical input angles. The central plane of the upper unit twists by an angle of α_C' with respect to the central plane of the bottom unit, which is fixed to the ground. The twisting motion and the transformation process are presented in Fig. 3(a) to 3(d), corresponding to the actuation angle, θ, of 0°, 30°, 60°, and 90°, respectively. The twisting angle, α_C', increases gradually from 0° to 60°. It should be noted that the upper central plane keeps parallel to the bottom central plane in the transformation process in the model.

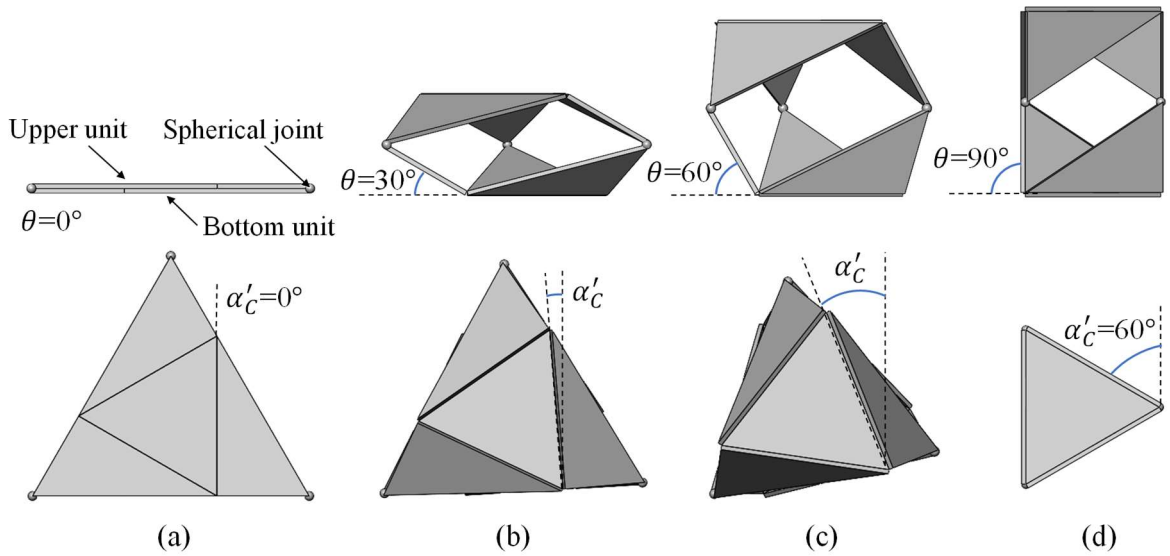


Fig. 3. 3D model of the primary design of the helical origami mechanism (with spherical joints) and its transformation process with the input angles of (a) $\theta = 0^{\circ}$; (b) $\theta = 30^{\circ}$, (c) $\theta = 60^{\circ}$; and (d) $\theta = 90^{\circ}$. (Three input angles are identical.)

The number of total components of this structure (N) is 8. Crease lines are considered as equivalent rotational joints and the number, n, is 6. The number of spherical joints, m, is 3. Therefore, the DoF of this helical origami mechanism with three spherical joints can be easily determined based on the Gruebler's criterion as follows:

$$\mathrm{DoF} = 6 \times (N - 1) - n \times (6 - 1) - m \times (6 - 3) = 3 \quad (5)$$

However, the traditional spherical joints do not exist in the origami field. The function of the spherical joints should be achieved by alternative 3-hinged origami joints to perform the desired helical motion and fabricate origami robots based on this kinematic design.

3.2 The New Helical Mechanism with 3-hinged Origami Connecting Joint

A spherical joint enables three rotational motions that are perpendicular to each other. It can be replaced by three rotational joints with axes intersecting with each other from the perspective of equivalent DoF [46]. The three rotational joints are connected in series by extra panels as illustrated in Fig. 4, which satisfies the origami principles. However, the introduced two extra panels of each connecting position increase the total number of components in the origami robot mechanism. The 3D model of the helical origami mechanism with alternative 3-hinged origami joints and its transformation

process with different actuation angles is illustrated in Fig. 5. The twisting motion of the upper central plane is successfully achieved in this 3D model and the helical origami mechanism can be fabricated in a purely-origami manner.

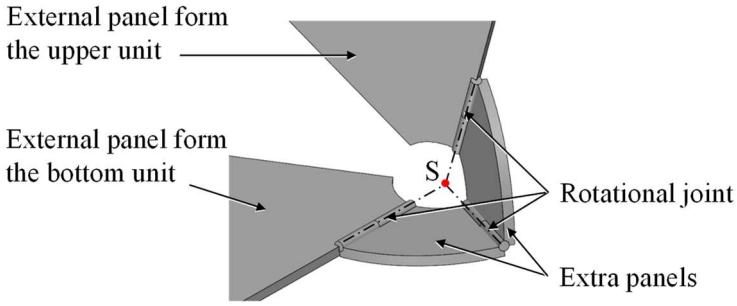


Fig. 4. An alternative 3-hingned origami joint following the origami principle with three rotational joints and two extra panels (equivalent to the traditional spherical joint).

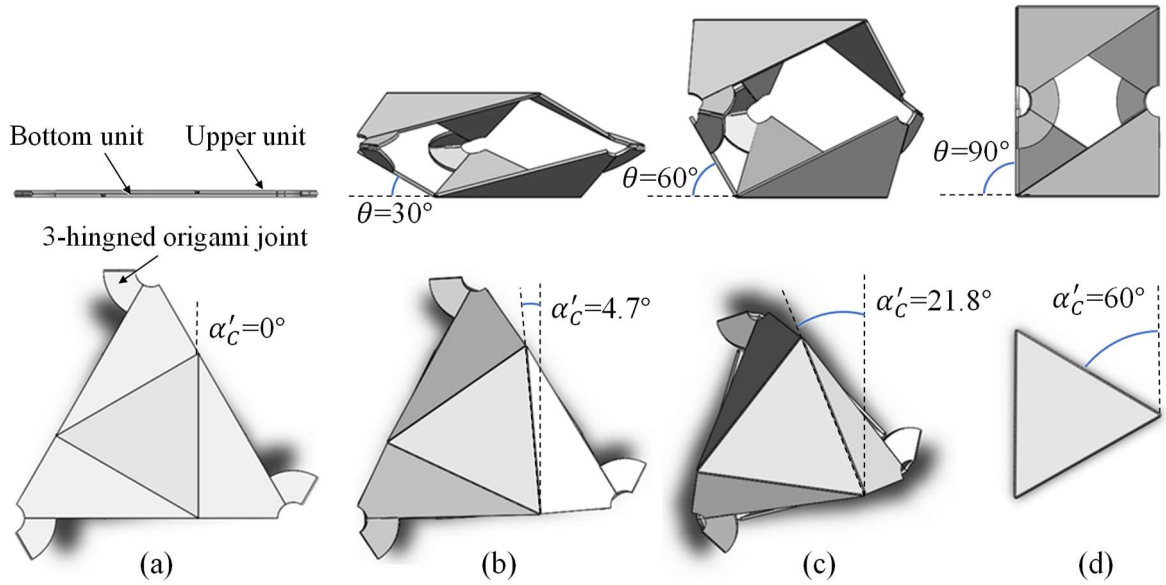


Fig. 5. The helical origami mechanism with alternative 3-hinged origami joints and its transformation process with the input angles of (a) $\theta = 0^{\circ}$; (b) $\theta = 30^{\circ}$, (c) $\theta = 60^{\circ}$; and (d) $\theta = 90^{\circ}$. (Three input angles are identical.)

The total number (N) of the helical origami mechanism with alternative 3-hinged origami joints (as shown in Fig. 5) is 14. All joints here are rotational joints and their number, n, is 15. The mobility of the helical origami mechanism remains three according to Eq. (6) based on Gruebler's criterion.

$$DoF = 6 \times (N - 1) - n \times (6 - 1) = 3 \tag{6}$$

The helical origami mechanism is composed of two minimum units arranged in a stack as shown in Fig. 5. Therefore, the twisting angle, α_C', and increase of the height, h_O, of the helical origami mechanism can be calculated by Eqs. (7) and (8), as follows based on Eqs. (2) and (3).

$$\alpha_C{}' = 120^{\circ} - 2\arctan\left(\frac{2\cos\omega t + 1}{\sqrt{3}}\right) \tag{7}$$

$$h_O = 2l \cdot \sin\omega t \tag{8}$$

In the overall transformation process, the origami robot mechanism shows helical motion as indicated in Fig. 5. It should be noted that the helical motion here is different from that of general screws. The ratio between the increase in height, h_O, and the twisting angle, α_C', is not constant during the twisting process, and it changes along with the actuating angle, θ, which is confirmed by Eqs. (7) and (8).

3.3 Kinematics Analysis of the Helical Origami Mechanism

The 3D model of the helical origami mechanism whose three external panels rotate with identical angles is shown in Fig. 6. The kinematic characteristics of the helical motion of this origami mechanism are analyzed based on the screw theory [27, 28, 47]. The three alternative 3-hinged origami joints (equivalent to traditional spherical joints) are marked as N, P and Q, respectively. The helical origami mechanism can also be seen as two central planes (i.e. ΔABC and ΔGHM) connected by three limbs (i.e. GH-N-BC, HM-P-AB and MG-Q-AC) in parallel. A global Cartesian coordinate frame O-XYZ is set up at the central plane of the bottom unit, ΔGHM, as indicated in Fig. 6. The origin of the coordinate, O, is coincident with the central point of the triangular plane. The X-axis is perpendicular to GH while Y-axis is parallel to GH. Z-axis is set through the right hand rule. The distance from O to GH is denoted by a, which is assumed as 1 for kinematic analysis in Fig. 6. In the limb 1, GH-N-BC, the screw of joint GH can be expressed as:

$$\mathrm{S_{GH}} = \left[0, 2\sqrt{3},\ 0,\ \ 0,\ \ 0,\ 2\sqrt{3}\right] \tag{9}$$

The screw of spherical joint N can be expressed as:

$$\mathrm{S_N} = \begin{cases} \left[1,\ 0,\ 0,\ 0,\ 2\sin\theta,\ -\sqrt{3}\right]^{\mathrm{T}} \\ [0,\ 1,\ 0, -2\sin\theta,\ 0,\ 2\cos\theta + 1]^{\mathrm{T}} \\ [0,\ 0,\ 1, -\sqrt{3},\ -(2\cos\theta + 1), 0]^{\mathrm{T}} \end{cases} \tag{10}$$

A local Cartesian coordinate frame o′- x′y′z′ is set up at the top plate ΔABC where the origin of the coordinate is coincident with the central point of the plane. x′-axis is perpendicular to BC while y′-axis is parallel to BC. z′-axis follows right hand rule. The screw of joint BC expressed in the local coordinate is:

$$\mathrm{o'_{S_{BC}}} = [0, 2\sqrt{3},\ 0,\ \ 0,\ \ 0,\ 2\sqrt{3}]^{\mathrm{T}} \tag{11}$$

The transformation matrix from local coordinate to global coordinate is:

$$\mathrm{O_{R_{o'}}} = \begin{bmatrix} \cos\delta & -\sin\delta & 0 & 0 & 0 & 0 \\ \sin\delta & \cos\delta & 0 & 0 & 0 & 0 \\ 0 & 0 & 0 & 0 & 0 & 0 \\ -4\sin\delta\sin\theta & -4\cos\delta\sin\theta & 0 & \cos\delta & -\sin\delta & 0 \\ 4\cos\delta\sin\theta & -4\sin\delta\sin\theta & 0 & \sin\delta & \cos\delta & 0 \\ 0 & 0 & 0 & 0 & 0 & 0 \end{bmatrix} \tag{12}$$

where δ is the rotational angle from global coordinate O-XYZ to local coordinate o'-x'y'z':

$$\delta = \pi - 2\arctan\left[(2\cos\theta + 1)/\sqrt{3}\right] \tag{13}$$

The screw of joint BC expressed in the global coordinate is:

$$\mathrm{S_{BC}} = \mathrm{O_{R_o}},\ \mathrm{o'_{S_{BC}}} = [-2\sqrt{3}\sin\delta,\ 2\sqrt{3}\cos\delta, 0, -8\sqrt{3}\cos\delta\sin\theta,\ -8\sqrt{3}\sin\delta\sin\theta,\ 0]^{\mathrm{T}} \tag{14}$$

The motion screws of limb 1 are:

$$S_1 = \begin{cases} \mathrm{S}_{11} = [0, 2\sqrt{3}, 0, 0, 0, 2\sqrt{3}]^{\mathrm{T}} \\ \mathrm{S}_{12} = [1, 0, 0, 0, 2\sin\theta, -\sqrt{3}]^{\mathrm{T}} \\ \mathrm{S}_{13} = [0, 1, 0, -2\sin\theta, 0, 2\cos\theta + 1]^{\mathrm{T}} \\ \mathrm{S}_{14} = [0,\ 0,\ 1, -\sqrt{3}, -(2\cos\theta + 1), 0]^{\mathrm{T}} \\ \mathrm{S}_{15} = [-2\sqrt{3}\sin\delta,\ 2\sqrt{3}\cos\delta, 0, -8\sqrt{3}\cos\delta\sin\theta, -8\sqrt{3}\sin\delta\sin\theta,\ 0]^{\mathrm{T}} \end{cases} \tag{15}$$

The constraint screw of limb 1 is:

$$\begin{aligned} \mathrm{S}_1^r = [\cot\theta, -2\cot\delta\cot\theta - \frac{1}{2}\left(\sqrt{3} + \cot\delta\right)\csc\theta, 1, 2\sqrt{3} + \cot\delta + 4\cos\theta\cot\delta, -1, -(3 \\ + 4\cos\theta)\cot\delta\cot\theta - \frac{1}{2}\left(\sqrt{3} + \cot\delta\right)\csc\theta]^{\mathrm{T}} \end{aligned} \tag{16}$$

The constraint screws of limbs 2, and 3 can be derived by rotating the screw vector S_1^r along Z axis by $\beta = 2\pi/3$, π and $4\pi/3$, respectively.

$$\mathrm{S}_k^r = \mathrm{R}_1\mathrm{S}_1^r \tag{17}$$

$$\mathrm{R}_1 = \begin{bmatrix} \cos\beta & -\sin\beta & 0 & 0 & 0 & 0 \\ \sin\beta & \cos\beta & 0 & 0 & 0 & 0 \\ 0 & 0 & 0 & 0 & 0 & 0 \\ 0 & 0 & 0 & \cos\beta & -\sin\beta & 0 \\ 0 & 0 & 0 & \sin\beta & \cos\beta & 0 \\ 0 & 0 & 0 & 0 & 0 & 0 \end{bmatrix} \tag{18}$$

The constraint-screw system employed on top plate is then derived as:

$$\mathrm{S}_{\mathrm{t}}^{\mathrm{r}} = \begin{cases} \mathrm{S}_1^{\mathrm{r}} = [\cot\theta, -2\cot\delta\cot\theta - \frac{1}{2}\left(\sqrt{3} + \cot\delta\right)\csc\theta, 1, 2\sqrt{3} + \cot\delta + 4\cos\theta\cot\delta, -1, \\ \qquad -(3 + 4\cos\theta)\cot\delta\cot\theta - \frac{1}{2}\left(\sqrt{3} + \cot\delta\right)\csc\theta]^{\mathrm{T}} \\ \mathrm{S}_2^{\mathrm{r}} = [-\frac{\cot\theta}{2} - \frac{\sqrt{3}}{2}\left(-2\cot\delta\cot\theta - \frac{1}{2}\left(\sqrt{3} + \cot\delta\right)\csc\theta\right), \frac{\sqrt{3}}{2}\cot\theta + \frac{1}{2}\left(2\cot\delta\cot\theta + \frac{1}{2}\left(\sqrt{3} + \cot\delta\right)\csc\theta\right), \\ \qquad 1, -\frac{\sqrt{3}}{2} + \frac{1}{2}(-\cot\delta - 4\cot\delta\cos\theta), \\ \qquad \frac{7}{2} + \frac{\sqrt{3}}{2}(\cot\delta + 4\cos\theta\cot\delta), -(3 + 4\cos\theta)\cot\delta\cot\theta - \frac{1}{2}(\sqrt{3} + \cot\delta)\csc\theta]^{\mathrm{T}} \\ \mathrm{S}_3^{\mathrm{r}} = [-\frac{\cot\theta}{2} + \frac{\sqrt{3}}{2}\left(-2\cot\delta\cot\theta - \frac{1}{2}\left(\sqrt{3} + \cot\delta\right)\csc\theta\right), -\frac{\sqrt{3}}{2}\cot\theta + \frac{1}{2}\left(2\cot\delta\cot\theta + \frac{1}{2}\left(\sqrt{3} + \cot\delta\right)\csc\theta\right), \\ \qquad 1, -\frac{3\sqrt{3}}{2} + \frac{1}{2}(-\cot\delta - 4\cot\delta\cos\theta), \\ \qquad \frac{5}{2} + \frac{\sqrt{3}}{2}(\cot\delta + 4\cos\theta\cot\delta), -(3 + 4\cos\theta)\cot\delta\cot\theta - \frac{1}{2}(\sqrt{3} + \cot\delta)\csc\theta]^{\mathrm{T}} \end{cases} \tag{19}$$

The motion-screw system of the top plate is then obtained as:

$$\mathrm{S}_{\mathrm{t}} = \begin{cases} \mathrm{S}_{\mathrm{t}1} = [0, 0, 1, 0, 0, \frac{(7 + 4\cos\theta + 5\cos 2\theta + 2\cos 3\theta)\csc\theta}{2\sqrt{3}}]^{\mathrm{T}} \\ \mathrm{S}_{\mathrm{t}2} = [0, 1, 0, -2\sin\theta - \frac{6(\sin\theta + \sin 2\theta)}{27 + 42\cos\theta + 29\cos 2\theta + 12\cos 3\theta + 4\cos 4\theta}, \\ \qquad -\frac{2\sqrt{3}(1 + 2\cos\theta)^2(1 + 4\cos\theta)\sin\theta}{27 + 42\cos\theta + 29\cos 2\theta + 12\cos 3\theta + 4\cos 4\theta}, 0]^{\mathrm{T}} \\ \mathrm{S}_{\mathrm{t}3} = [1, 0, 0, -\frac{2\sqrt{3}(1 + 2\cos\theta)^2(1 + 4\cos\theta)\sin\theta}{27 + 42\cos\theta + 29\cos 2\theta + 12\cos 3\theta + 4\cos 4\theta}, \\ \qquad 2\sin\theta + \frac{6(\sin\theta + \sin 2\theta)}{27 + 42\cos\theta + 29\cos 2\theta + 12\cos 3\theta + 4\cos 4\theta}, 0]^{\mathrm{T}} \end{cases} \tag{20}$$

Based on the Eq. (20), the pitch of the helical motion of the helical origami mechanism along Z-axis is:

$$Pitch = \frac{(7 + 4\cos\theta + 5\cos 2\theta + 2\cos 3\theta)\csc\theta}{2\sqrt{3}} \tag{21}$$

It is indicated in Eq. (20) that the helical origami mechanism has three DoFs and is able to achieve pure helical motion with a variable pitch when the three external panels of the bottom unit bend simultaneously with the identical initial angle and angular speed. The relationship between the pitch and the input angles is plotted in Fig. 7 based on Eq. (21) under the condition of particular design parameters. The pitch curve corresponding to the actuation angles close to 0° indicates that the origami mechanism has a large pitch and the translational motion dominates in this actuation angle range. By contrast, the pitch curve corresponding to the actuation angles close to 90° indicates a small pitch and the twisting motion of the origami mechanism dominates in this actuation angle range. This variable pitch makes the helical origami mechanism less suitable for the application scenarios related to traditional helical motions and screws with constant pitches. However, it enables the helical origami mechanism to achieve tasks where the translational motion is more required at the beginning/end and the twisting motion is more expected at the end/beginning. In addition, the variable pitch curve can be further modified by changing the design parameters based on certain particular applications.

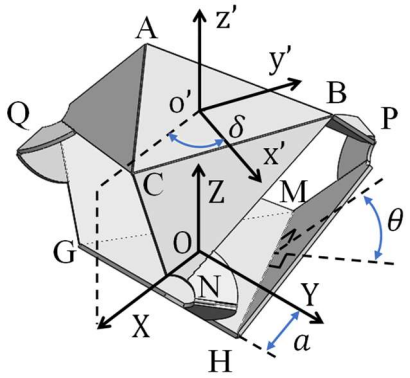


Fig. 6. Schematic model of the helical origami mechanism for kinematic analysis.

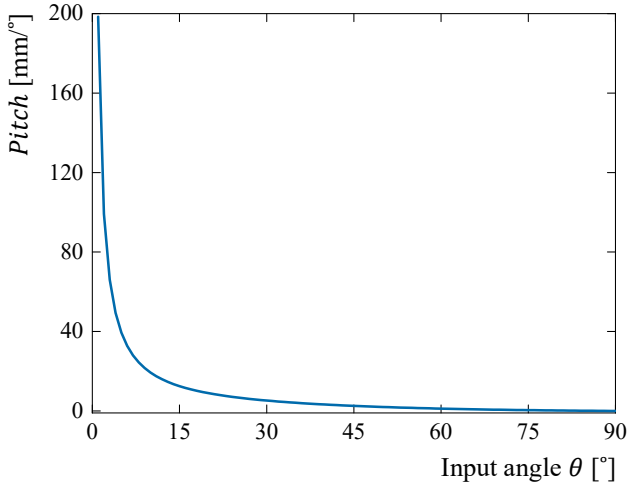


Fig. 7. Pitch of the helical origami mechanism ($a = 1$ mm).

In this case, the top central plane is parallel to the bottom central plane in the whole moving process. The derived equations indicate that the helical motion is controllable and programmable. For practical interests that only helical motion is needed, we can add a simple cylindrical constraint to the end effector of the mechanism [48]. Such a mechanism (with a central cylindrical constriction and a single

actuation input) and its transformation process are schematically shown in Fig. 8. By doing this, the mobility reduces to one that can be controlled easily using one actuation without a need to synchronise input from three actuators. This is advantageous to the application of this helical only motion of the origami mechanism.

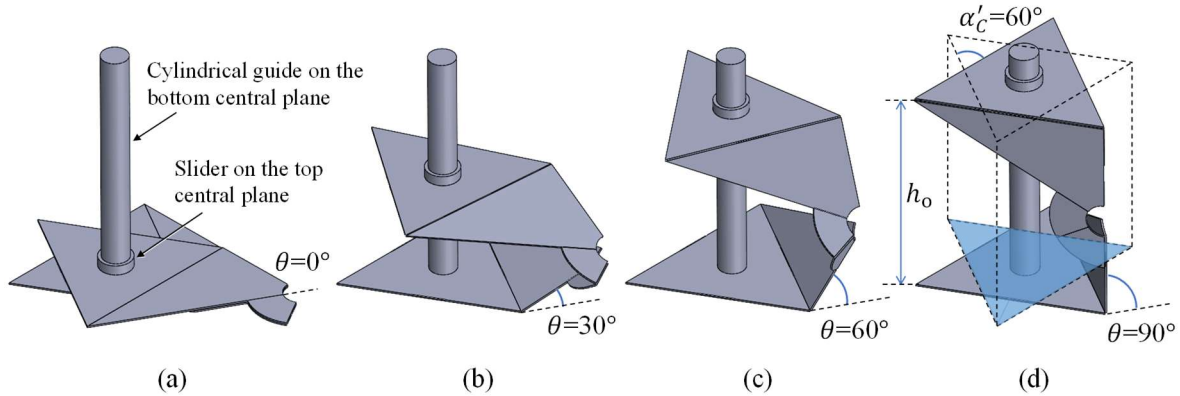


Fig. 8. A helical mechanism (with a central cylindrical constriction and a single actuation input) and its transformation process with the input angle of (a) $\theta = 0^{\circ}$; (b) $\theta = 30^{\circ}$, (c) $\theta = 60^{\circ}$; and (d) $\theta = 90^{\circ}$.

3.4 Workspace of the Helical Origami Mechanism

According to the schematic model of the Helical origami mechanism, we have

$$\mathrm{H} = [1, \sqrt{3}, 0] \times a \tag{22a}$$
$$\mathrm{M} = [-2,0,0] \times a \tag{22b}$$
$$\mathrm{G} = [1, -\sqrt{3,0}] \times a \tag{22c}$$
$$\mathrm{N} = [1 + 2\cos\theta_1, \sqrt{3}, 2\sin\theta_1] \times a \tag{22d}$$
$$\mathrm{P} = [-2 - \cos\theta_2, \sqrt{3\cos\theta_2}, 2\sin\theta_2] \times a \tag{22e}$$
$$\mathrm{Q} = [1 - \cos\theta_3, -\sqrt{3} - \sqrt{3\cos\theta_3}, 2\sin\theta_3] \times a \tag{22f}$$

θ_i (i=1,2 and 3) is any of the three inputs.

The positions of points A, B and C can be set as

$$\mathrm{A} = (x_1, y_1, z_1) \tag{23a}$$
$$\mathrm{B} = (x_2, y_2, z_2) \tag{23b}$$
$$C = (x_3, y_3, z_3) \tag{23c}$$

The centre of the top platform of helical origami mechanism o' is calculated by

$$\mathrm{o'} = (x, y, z) = \frac{\mathrm{A} + \mathrm{B} + \mathrm{C}}{3} \tag{24}$$

Here are nine geometric constraints for the helical origami mechanism:

$$\mathrm{AB} = \mathrm{BC} = \mathrm{AC} = 2\sqrt{3}a \tag{25a}$$
$$\mathrm{CN} = \mathrm{BP} = \mathrm{AQ} = 2a \tag{25b}$$
$$\mathrm{BN} = \mathrm{AP} = \mathrm{CQ} = 4a \tag{25c}$$

As the number of unknown parameters about points A, B and C is equal to the number of geometric constraints, the workspace of the centre point o' of the helical origami mechanism can be calculated. When the all the inputs θ_i change in the rotational range of [0° , 90°], the result of a sample with scale factor $a = 10\sqrt{3}$ mm is shown in Fig. 9.

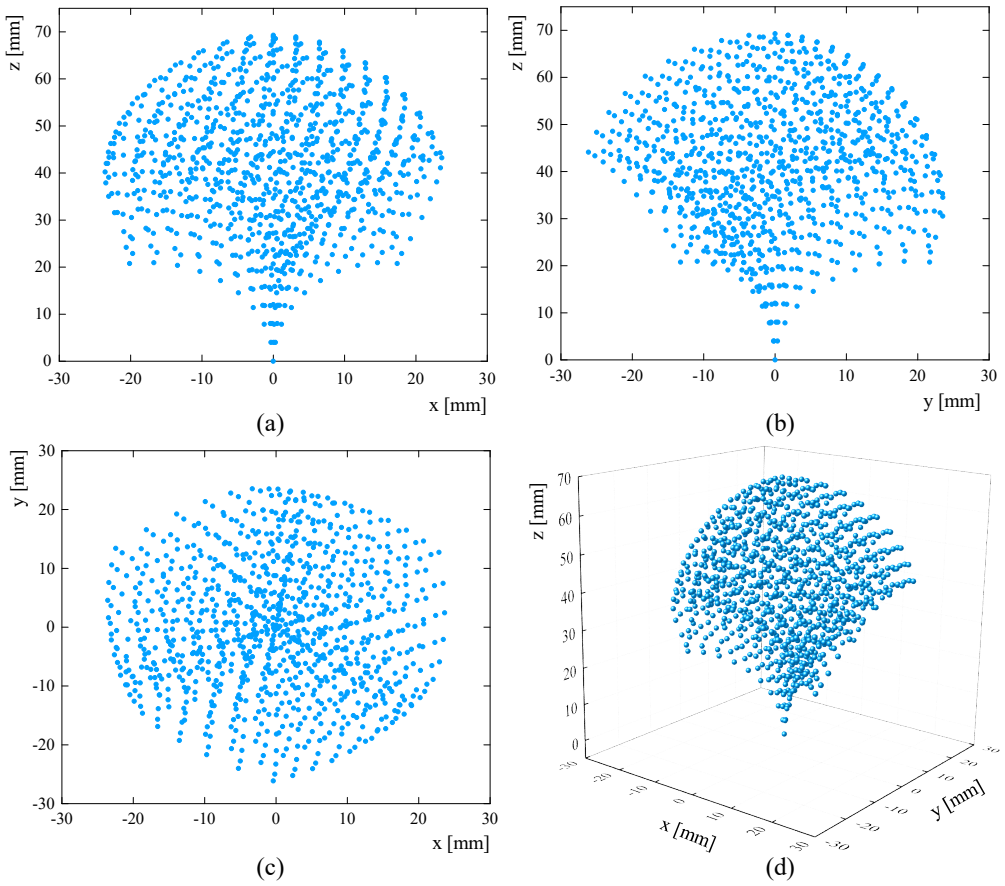


Fig. 9. Workspace of the centre point o′ of the helical origami mechanism. (a) View along y-axis; (b) View along x-axis; (c) View along z-axis; (d) Isometric view.

It is shown in Fig. 9 that the x coordinate of the centre o′ ranges from -23.5771 mm to 23.6226 mm. The y coordinate of the centre o′ ranges from -26.1413 mm to 23.6051 mm. The z coordinate of the centre o′ ranges from 0 mm to 69.2820 mm.

The classical 3-RSR mechanisms, either in the origami forms or not, can also achieve diverse spatial motion configurations, while the helical motion is not available. Compared with these classical 3-RSR mechanisms. this novel origami mechanism is capable of the helical motion and diverse motion configurations corresponding to different actuation angles. This is the main advantage of this design. In addition, no flexible panel exists in this origami mechanism. Rigid materials can be used in the fabrication for a higher structural strength.

4 Prototype Fabrication and Experimental Test

The crease pattern is obtained and presented in Fig. 10 when the helical origami mechanism is completely unfolded. When the bottom or top central plane is divided into three equal parts from the central point, a fan-shape crease pattern is obtained (as shown in Fig. 10(a)) in this case. It should be noted that the crease pattern shown in Fig. 10(a) is one example of many possible solutions. The dotted lines represent valley folds while the solid lines represent the mountain folds and outlines. Based on this pattern, we can easily fabricate a helical origami mechanism from foldable materials in sheets. Connecting operation is still required in certain positions to complete the fabrication. This monolithic character of the origami robot mechanism highly reduces fabrication time and cost. In addition,

foldable materials in thin-sheet forms, such as membranes, steel, plastic, and carbon fibre plastic composites, can be used for the fabrication of the mechanism for different application scenarios.

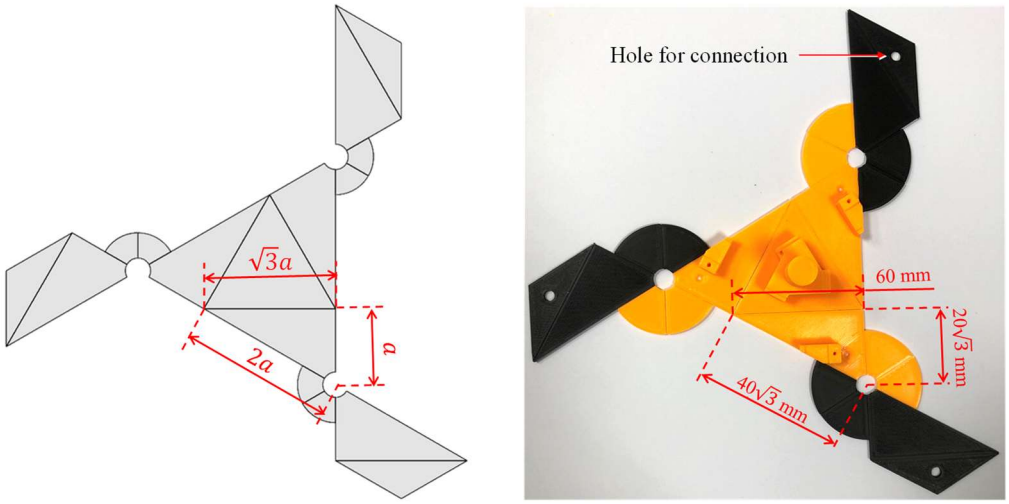


Fig. 10. (a) The crease patterns of the helical origami mechanism; and (b) The completely unfolded prototype fabricated using 3D printing.

Based on the crease pattern shown in Fig. 10(a), a prototype is fabricated using 3D printing and the material is PLA. The crease pattern of the fully unfolded prototype is shown in Fig. 10(b). The hole on each lamb of this fan-shape prototype is for connection and to form the complete upper central panel of the helical origami mechanism. The key dimensions of the prototype are indicated in Fig. 10(b) and the thickness is 2 mm. Every two adjacent plates are connected by adhesive tapes and the rotational joints (i.e. mountain fold and valley fold) are naturally formed. The completed prototype is shown in Fig. 11(a). It should be highlighted that 3 redundant equivalent spherical joints are introduced in the prototype to enhance the strength of the prototype. However, they do not influence on the kinematic characteristics of the helical origami mechanism.

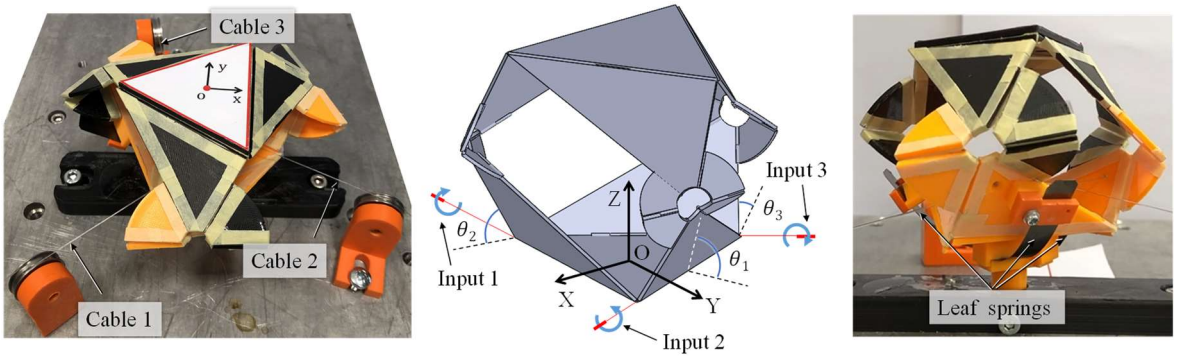


Fig. 11. (a) The helical origami mechanism prototype actuated by 3 cables; (b) Arrangement of the three inputs; (c) Distribution of the leaf springs which provide force against actuation.

This helical origami mechanism is actuated by cables [49]. Three actuation angles, θ_i $(i = 1, 2, 3)$, of external panels of the bottom unit determine the helical behavior and diverse spatial configurations of the origami robot mechanism. They are also corresponding to the 3 DoFs of the design. The arrangement of the three inputs which fold the three bottom external panels with respect to the crease lines is illustrated in Fig. 11(b). The range for each actuating angle is set to be from 0° to 90° to avoid interference of the planes. Other possible actuating methods include shape memory alloy [23],

pneumatic actuators [31], and etc. Three leaf springs (as indicated in Fig. 11(c)) are utilized in this mechanism. One end of each leaf spring is fixed on the bottom central panel (the base). The other side of the leaf spring can slide along the guide attached to the bottom external panels. These leaf springs provide force against actuation (folding of the bottom external panels) and help the helical origami mechanism go back to the original configuration (where $\theta_i = 0°$) when the cables are released. Singularity and bifurcation are avoided in this prototype. This is because joints (formed by adhesive tapes) only exist on one side of the panels. The thickness of the panels prevents the joints rotate over 180°. In addition, the leaf springs give a folding tendency of the bottom external panels. This also helps to eliminate the singularity and bifurcation in the working process.

It should be noted that this origami prototype twists in the clockwise direction which is opposite to the direction presented in Fig. 5. This is due to the different arrangement patterns of the central panels and the external panels in the prototype, which are symmetric to the pattern in Fig. 5. This feature provides an easy approach to designing the helical origami mechanisms with different twisting angular directions. However, the numerical relationship between the input angles and output angles and heights is not influenced.

The helical motion of the origami mechanism is experimentally investigated using the prototype. The folding motion of the bottom external panels is manually motivated through the cables. The three input folding angles, θ_i $(i = 1, 2, 3)$, are controlled and kept identical by reference blocks with standard angles. The transformation process of the prototype corresponding to the input angle, θ, of 0°, 30°, 60° and 90° are shown in Fig. 12, respectively. The twisting motion of the upper central panel and the increase of the height of the origami mechanism are observed.

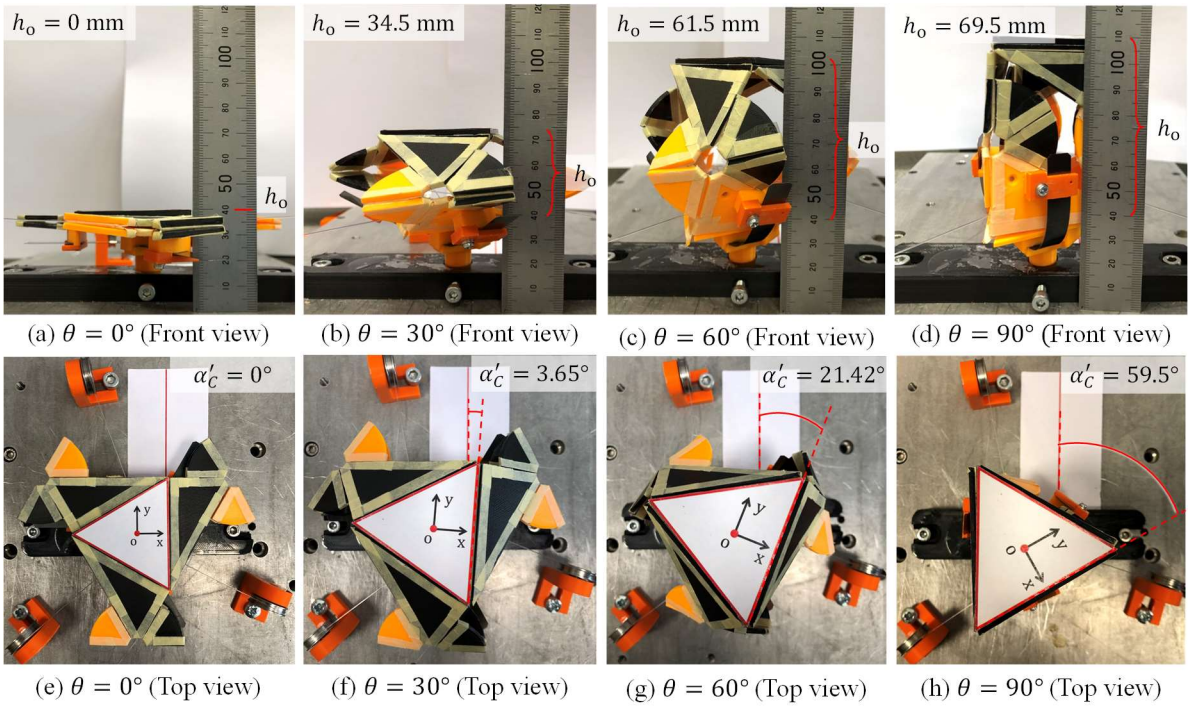


Fig. 12. The transformation process of the prototype corresponds to the input angle, θ, of 0°, 30°, 60° and 90°. (The continuous twisting motion is recorded and presented in the video available through the link in Appendix.)

The output twisting angle, α'_C, of the top central panel and the height, h_o, of the origami mechanism are measured in the experiments. The experimental results and the theoretical results based on Eqs. (7)

and (8) are plotted and compared in Fig. 13. A close agreement is observed. The maximum absolute error of the twisting angle, α'_C, is 2.9° and it is observed when the input folding angle, θ, is 75°. The root mean square error is 1.21°. The error of the height of the origami mechanism reaches a maximum of 1.9 mm when the input folding angle, θ, is 15°. The root mean square error is 1.08 mm. Errors are from multiple sources which include measurement inaccuracy, assembling errors, enlarged gaps between the panels due to the changing adhesive condition of the tapes over time, etc. The twisting behaviour of the top plate and the overall helical motion, which are theoretically analysed in Section 3, are experimentally verified.

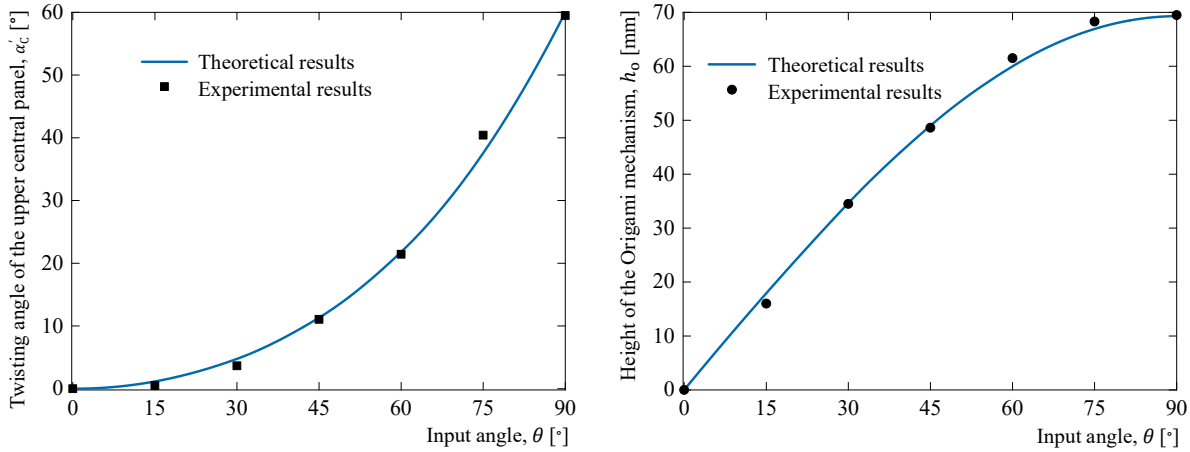


Fig. 13. Experimental and theoretical results of (a) the twisting angle of the upper central panel, α'_C, and (b) The height of the origami mechanism, h_O, with respect to the input angle, θ.

5 Motion Configurations and an Extended Multi-Module Mechanism

The helical origami mechanism proposed has 3 DoFs based on the kinematic analysis. The helical motion around the Z-axis (in the coordinate system in Fig. 6), is achieved with three identical input angles changing simultaneously at the same speed. This helical motion around the Z axis is just one of the three possible motions. Due to the 3 DoFs of the design, diverse motion configurations can be achieved with different settings of input angles.

5.1 Diverse Motion Configurations

General motion configurations of this helical origami mechanism include coupled twisting and translation motions in space. Several motion configurations with different combinations of input angles are demonstrated in Figs. 14-17 using both the 3D model and the prototype for comparison. They are presented as examples of possible spatial configurations and reachable positions. It is shown that the origami robot mechanism can reach a large range of spatial positions defined by the workspace in Fig. 9 with diverse orientations. The spatial motion configurations of the 3D model and the prototype match well with the same set of input angles. The minor difference could be caused by the imperfection of the joints formed by adhesive tapes. The spatial motion configurations can be decomposed into three twisting motions about the perpendicular axes of the coordinate system in Fig. 6 coupling with three translational motions along the axes. Alternatively, the three translational motions along the axes can be regarded as primary motions while the twisting motions about the three axes are coupling motions.

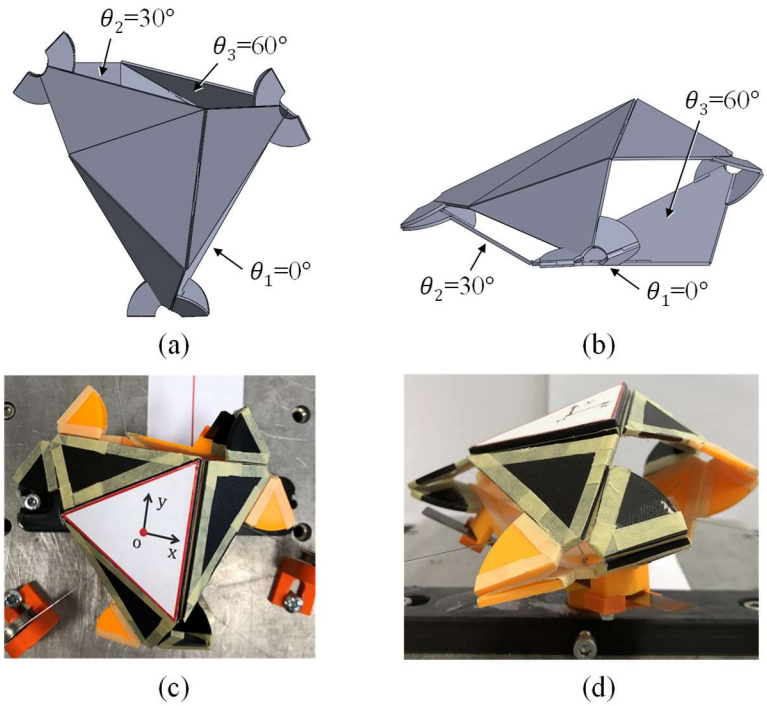


Fig. 14. Motion configuration of the helical origami mechanism with input angles: θ_1=0°, θ_2=30°, θ_3=60°. (a) Top and (b) Front views of the 3D model; (c) Top and (d) Front views of the prototype.

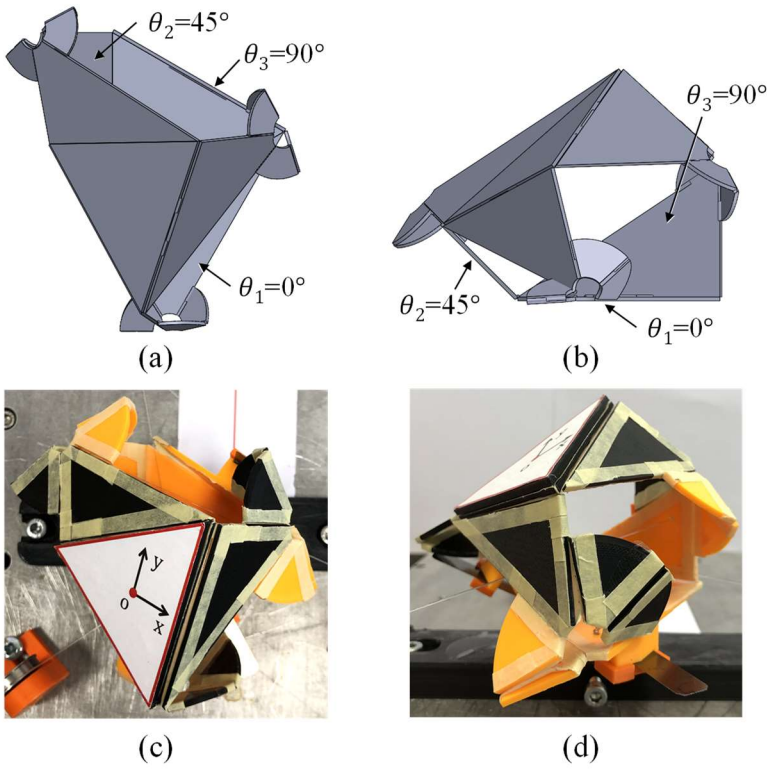


Fig. 15. Motion configuration of the helical origami mechanism with input angles: θ_1=0°, θ_2=45°, θ_3=90°. (a) Top and (b) Front views of the 3D model; (c) Top and (d) Front views of the prototype.

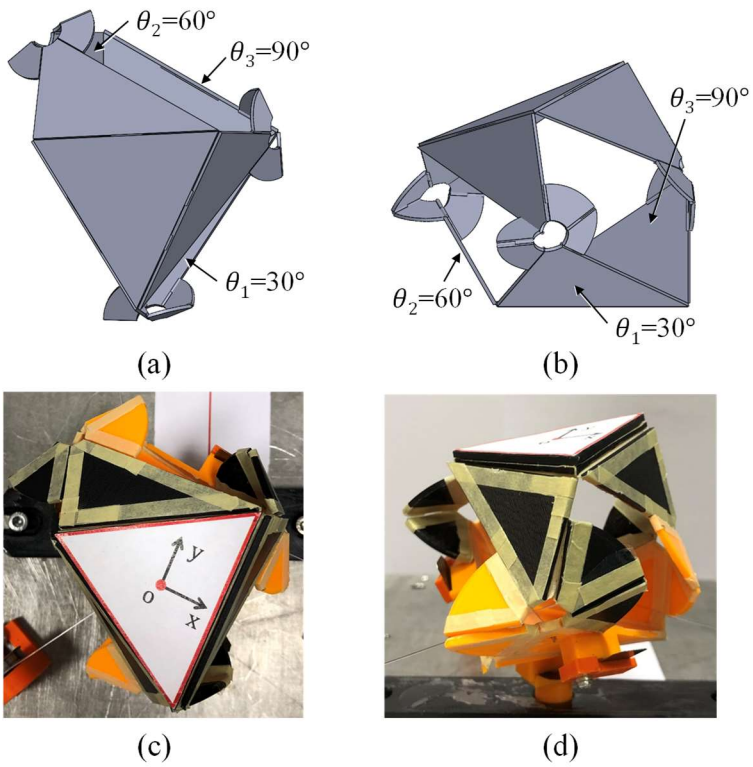


Fig. 16. Motion configuration of the helical origami mechanism with input angles: θ_1=30°, θ_2=60°, θ_3=90°. (a) Top and (b) Front views of the 3D model; (c) Top and (d) Front views of the prototype.

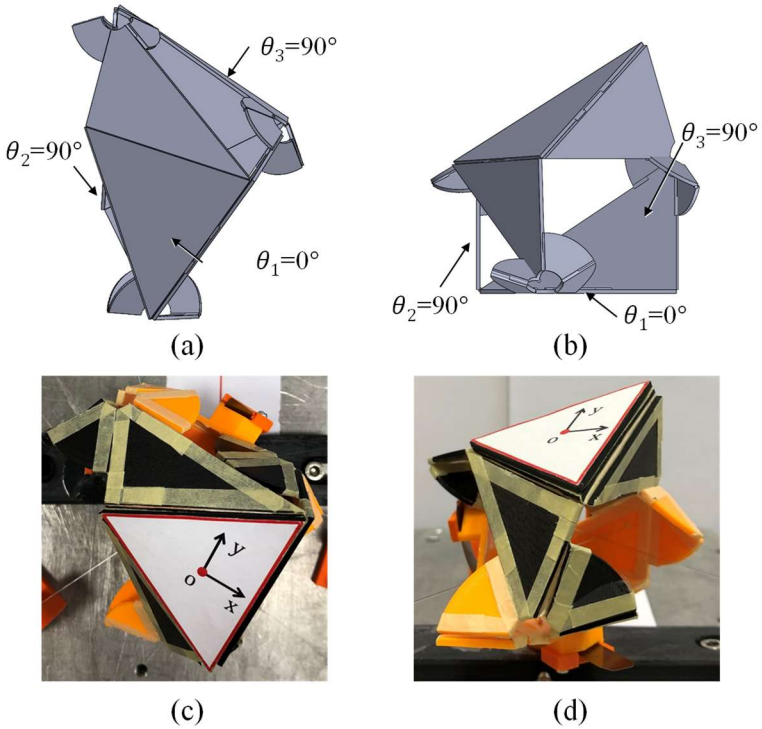


Fig. 17. Motion configuration of the helical origami mechanism with input angles: θ_1=0°, θ_2=90°, θ_3=90°. (a) Top and (b) Front views of the 3D model; (c) Top and (d) Front views of the prototype.

5.2 An Integrated Robot Connecting Helical Origami Mechanisms in Series

A more complex continuous origami robot is proposed in this section where a helical origami mechanism is regarded as a construction module. This is achieved by integrating a couple of modules in series for a larger twisting angle and a wider operating range. An example of such an integrated origami robot mechanism is shown in Fig. 18. The main challenge here is actuating the complex device with a minimum number of actuators. This problem can be solved mechanically by using well-designed origami links as indicated in Fig. 18(a). Each origami link contains two extra panels and three rotational joints, forming a four-bar link together with one external panel from the upper unit of the bottom helical origami mechanism (Helical module 2) and another external panel from the bottom unit of the upper helical origami mechanism (Helical module 1). In this way, the integrated origami robot still has 3 DoFs and only three actuators are required to achieve desired motions. One transformation configuration of this integrated robot from different perspectives is shown in Fig. 18(a) to (d). Its unfolded mode, where all three actuating angles are zero, is shown from the top view in Fig. 18(e). In this mode, the continuous robot has a minimum volume.

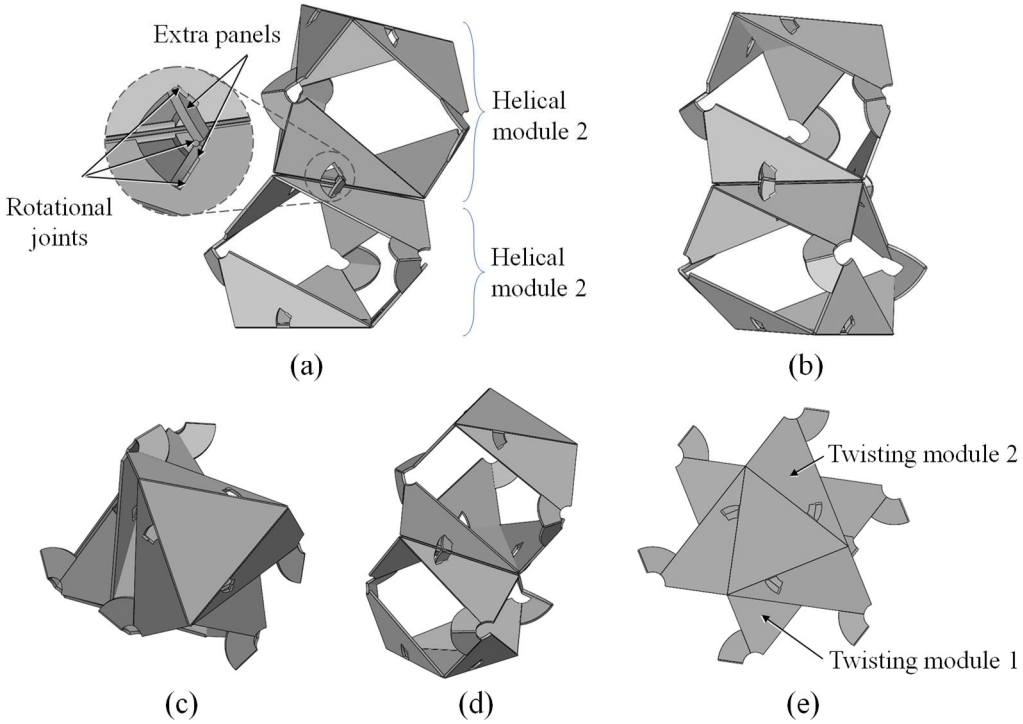


Fig. 18. Integrated origami robot connecting two helical origami mechanism in series and its transformation configuration from different perspectives.

6 Conclusions

The minimum units of Resch Triangular Tessellation show twisting behaviour during the folding process. Inspired by this origami tessellation, a helical origami mechanism was designed by connecting two minimum units in a stack face to face. Specially designed alternative 3-hinged origami joints which are equivalent to traditional spherical joints, are adopted for connection. By rotating the panels connected to the triangular base, the origami mechanism implements various motions. The top central panel twists for 60˚ and remained parallel with respect to the bottom base when all three adjacent panels rotate 90˚ simultaneously with the identical angular displacement. This helical motion was confirmed by the kinematic analysis based on the screw theory. According to the geometric

analysis, equations describing the twisting angle and the height increase of the origami robot mechanism were derived. It is shown that the top central panel of the helical origami mechanism traces a nonlinear helical motion with a variable pitch. The workspace of the centre point, o', of the helical origami mechanism is also derived and presented. The helical motion was experimentally verified by using the proof-of-the-concept prototype which is actuated by cables.

The helical origami mechanism demonstrated in this study has three DoFs. The helical motion (i.e. twisting motion coupled with the vertical translation) is one of the three available motion configurations, which can be achieved by controlling the three input angles θ_i $(i = 1, 2, 3)$. Based on the 3D model and the prototype, diverse possible motion configurations corresponding to different settings of actuating angles were illustrated from multiple perspectives. Taking the helical origami mechanism as a module, an integrated origami mechanism was proposed by connecting a couple of the helical modules in series. The integrated origami mechanism amplified the twisting angles and reachable range. The number of required actuators for this integrated origami robot remained a minimum of three by using the 3-hinged origami connecting joints. The controllable diverse motions (translation and twisting) with 3 DoFs distinguish the helical origami mechanism from the existing origami structures in literature.

Main contributions of this research are summarized as follows.

- An origami-based mechanism capable of helical motion with identical input angles is proposed in this study. Diverse spatial motion configurations are also achievable with the same device corresponding to different input angles. Such a structure is reported for the first time based on the authors' knowledge.
- The kinematic model of this helical origami mechanism is established and a cable-actuated prototype is successfully fabricated. All these provide a basis for the future applications and further research of this novel origami mechanism.

This helical origami mechanism shows multiple advantages including the controllable and programmable helical motion, diverse motion configurations through simple folding operations, ultra-compact original volume, etc. Limitations of this helical origami mechanism exist. Firstly, the twisting angle of the top central plane reaches its maximum limit of 60˚ corresponding to the actuation angle of 90˚ due to the intrinsic geometric relationship. A larger twisting angle is not available with a single helical origami mechanism in the actuation angle range from 0˚ to 90˚. In addition, translational or twisting motion only cannot be achieved with a single helical origami mechanism. Potential application scenarios include surgical manipulators in minimally invasive surgery [50], soft robotic arms [51], pointers in spacecraft [52], 3-DoF operation platforms, search and rescue, scenarios where helical motions are needed, etc. This helical origami mechanism can also be fabricated at various scales due to its scalability. Future research and development will be focused on the following aspects: kinematic analysis of all possible motions, development of an integrated robot with more helical modules, analysis and application of the helical motion with a variable pitch, etc.

Acknowledgements

This work was supported by the National Forum T&L Initiative Type 001/19 project (Linking origami Art in Robotics Education), the EU Horizon 2020 research & innovation programme EnABLES (grant

agreement no 730957), and The Royal Society Research Grant awarded to Dr Zhang (under the Grant Agreement No. RGS\R1\211326).

Appendix

The transformation process of this helical origami mechanism with identical and different input angles is presented in the video: https://youtube.com/shorts/N990ADcKARc.

References

[1] Tachi, T. Freeform origami tessellations by generalizing Resch's patterns. ASME 2013 International Design Engineering Technical Conferences and Computers and Information in Engineering Conference, 2013. American Society of Mechanical Engineers Digital Collection.
[2] Debnath, S. & Fei, L. 2013. Origami theory and its applications: a literature review. World Academy of Science, Engineering and Technology, 1131-1135.
[3] Demaine, E. D. Folding and unfolding linkages, paper, and polyhedra. Japanese Conference on Discrete and Computational Geometry, 2000. Springer, 113-124.
[4] Buri, H. & Weinand, Y. 2008. ORIGAMI-folded plate structures, architecture.
[5] Sorguç, A. G., Hagiwara, I. & Selcuk, S. 2009. Origamics in architecture: a medium of inquiry for design in architecture. Metu Jfa, 2, 235-247.
[6] Thrall, A. & Quaglia, C. 2014. Accordion shelters: A historical review of origami-like deployable shelters developed by the US military. Engineering structures, 59, 686-692.
[7] Hull, T. 2012. Project origami: activities for exploring mathematics, CRC Press.
[8] Hull, T. 1994. On the mathematics of flat origamis. Congressus numerantium, 215-224.
[9] Santangelo, C. D. 2020. Theory and practice of origami in science. Soft matter, 16, 94-101.
[10] Zirbel, S. A., Lang, R. J., Thomson, M. W., Sigel, D. A., Walkemeyer, P. E., Trease, B. P., Magleby, S. P. & Howell, L. L. 2013. Accommodating thickness in origami-based deployable arrays. Journal of Mechanical Design, 135.
[11] Edmondson, B. J., Bowen, L. A., Grames, C. L., Magleby, S. P., Howell, L. L. & Bateman, T. C. Oriceps: Origami-inspired forceps. ASME 2013 conference on smart materials, adaptive structures and intelligent systems, 2013. American Society of Mechanical Engineers Digital Collection.
[12] Dai, J. S. & Rees Jones, J. 1999. Mobility in metamorphic mechanisms of foldable/erectable kinds.
[13] Lang, R. J. 2011. Origami design secrets: mathematical methods for an ancient art, AK Peters/CRC Press.
[14] Kanade, T. 1980. A theory of origami world. Artificial intelligence, 13, 279-311.
[15] Peng, R., Ma, J. & Chen, Y. 2018. The effect of mountain-valley folds on the rigid foldability of double corrugated pattern. Mechanism and Machine Theory, 128, 461-474.
[16] Davis, E., Demaine, E. D., Demaine, M. L. & Ramseyer, J. 2013. Reconstructing David Huffman's origami tessellations. Journal of Mechanical Design, 135.
[17] Chen, Y., Yan, J. & Feng, J. 2019. Geometric and Kinematic Analyses and Novel Characteristics of Origami-Inspired Structures. Symmetry, 11, 1101.
[18] Faber, J. A., Arrieta, A. F. & Studart, A. R. 2018. Bioinspired spring origami. Science, 359, 1386-1391.
[19] Belke, C. H. & Paik, J. 2017. Mori: a modular origami robot. IEEE/ASME Transactions on Mechatronics, 22, 2153-2164.
[20] Miyashita, S., Guitron, S., Ludersdorfer, M., Sung, C. R. & Rus, D. An untethered miniature origami robot that self-folds, walks, swims, and degrades. 2015 IEEE International Conference on Robotics and Automation (ICRA), 2015. IEEE, 1490-1496.

[21] Mcclintock, H., Temel, F. Z., Doshi, N., Koh, J.-S. & Wood, R. J. 2018. The milliDelta: A high-bandwidth, high-precision, millimeter-scale Delta robot. Science Robotics, 3, eaar3018.
[22] Li, S., Stampfli, J. J., Xu, H. J., Malkin, E., Diaz, E. V., Rus, D. & Wood, R. J. A Vacuum-driven Origami "Magic-ball" Soft Gripper. 2019 International Conference on Robotics and Automation (ICRA), 2019. IEEE, 7401-7408.
[23] Hao, G., Yu, J. & Li, H. 2016. A brief review on nonlinear modeling methods and applications of compliant mechanisms. Frontiers of Mechanical Engineering, 11, 119-128.
[24] Nelson, T. G., Avila, A., Howell, L. L., Herder, J. L. & Machekposhti, D. F. 2019. Origami-inspired sacrificial joints for folding compliant mechanisms. Mechanism and Machine Theory, 140, 194-210.
[25] Zhang, K., Qiu, C. & Dai, J. S. 2016. An extensible continuum robot with integrated origami parallel modules. Journal of Mechanisms and Robotics, 8, 031010.
[26] Salerno, M., Zhang, K., Menciassi, A. & Dai, J. S. 2016. A novel 4-DOF origami grasper with an SMA-actuation system for minimally invasive surgery. IEEE Transactions on Robotics, 32, 484-498.
[27] Dai, J. S. & Jones, J. R. 2001. Interrelationship between screw systems and corresponding reciprocal systems and applications. Mechanism and machine theory, 36, 633-651.
[28] Dai, J. 2014. Geometrical foundations and screw algebra for mechanisms and robotics. Springer, London.
[29] Peraza-Hernandez, E. A., Hartl, D. J., Malak Jr, R. J. & Lagoudas, D. C. 2014. Origami-inspired active structures: a synthesis and review. Smart Materials and Structures, 23, 094001.
[30] Feng, H., Peng, R., Zang, S., Ma, J. & Chen, Y. 2020. Rigid foldability and mountain-valley crease assignments of square-twist origami pattern. Mechanism and Machine Theory, 152, 103947.
[31] Jiang, Z. & Zhang, K. A Novel Torsional Actuator Augmenting Twisting Skeleton and Artificial Muscle for Robots in Extreme Environments. 2021 IEEE International Conference on Robotics and Automation (ICRA), 2021. IEEE, 9318-9324.
[32] Zhang, K., Qiu, C. & Dai, J. S. 2015. Helical kirigami-enabled centimeter-scale worm robot with shape-memory-alloy linear actuators. Journal of Mechanisms and Robotics, 7, 021014.
[33] Kresling, B. 2012. Origami-structures in nature: lessons in designing "smart" materials. MRS Online Proceedings Library (OPL), 1420.
[34] Pagano, A., Yan, T., Chien, B., Wissa, A. & Tawfick, S. 2017. A crawling robot driven by multi-stable origami. Smart Materials and Structures, 26, 094007.
[35] Wu, S., Ze, Q., Dai, J., Udipi, N., Paulino, G. H. & Zhao, R. 2021. Stretchable origami robotic arm with omnidirectional bending and twisting. Proceedings of the National Academy of Sciences, 118.
[36] Berre, J., Geiskopf, F., Rubbert, L. & Renaud, P. 2022. Toward the Design of Kresling Tower Origami As a Compliant Building Block. Journal of Mechanisms and Robotics, 14, 045002.
[37] Moshtaghzadeh, M., Izadpanahi, E. & Mardanpour, P. 2021. Stability analysis of an origami helical antenna using geometrically exact fully intrinsic nonlinear composite beam theory. Engineering Structures, 234, 111894.
[38] Liu, X., Yao, S., Cook, B. S., Tentzeris, M. M. & Georgakopoulos, S. V. 2015. An origami reconfigurable axial-mode bifilar helical antenna. IEEE Transactions on Antennas and Propagation, 63, 5897-5903.
[39] Vander Hoff, E., Jeong, D. & Lee, K. OrigamiBot-I: A thread-actuated origami robot for manipulation and locomotion. 2014 IEEE/RSJ International Conference on Intelligent Robots and Systems, 2014. IEEE, 1421-1426.
[40] Jeong, D. & Lee, K. 2018. Design and analysis of an origami-based three-finger manipulator. Robotica, 36, 261-274.
[41] Yoneda, T., Matsumoto, D. & Wada, H. 2019. Structure, design, and mechanics of a paper spring. Physical Review E, 100, 013003.
[42] Cai, J., Ma, R., Feng, J., Zhou, Y. & Deng, X. 2016. Foldability analysis of cylindrical origami structures. Advances in Reconfigurable Mechanisms and Robots II. Springer.

[43] Wang, R., Zhou, X., Zhu, Z. & Liu, Q. 2015. Compliant linear-rotation motion transduction element based on novel spatial helical flexure hinge. Mechanism and Machine Theory, 92, 330-337.
[44] Resch, R. D. 1968. Self-supporting structural unit having a series of repetitious geometrical modules. Google Patents.
[45] Ghassaei., A. 2017. Origami Simulator [Online]. Available: http://apps.amandaghassaei.com/OrigamiSimulator/ [Accessed].
[46] Wang, R., Song, Y. & Dai, J. S. 2021. Reconfigurability of the origami-inspired integrated 8R kinematotropic metamorphic mechanism and its evolved 6R and 4R mechanisms. Mechanism and Machine Theory, 161, 104245.
[47] Zhang, K. & Dai, J. Reconfiguration analysis of wren platform and its kinematic variants based on reciprocal screw systems. Proceedings of the 14th IFToMM World Congress, 2015. 國立臺灣大學機械系, 237-242.
[48] Kiper, G. & Söylemez, E. Modified wren platforms. 13th IFToMM world congress, Guanojuato, Mexico, 2011.
[49] Zhang, Z., Tang, S., Fan, W., Xun, Y., Wang, H. & Chen, G. 2022. Design and analysis of hybrid-driven origami continuum robots with extensible and stiffness-tunable sections. Mechanism and Machine Theory, 169, 104607.
[50] Edmondson, B. J., Bowen, L. A., Grames, C. L., Magleby, S. P., Howell, L. L. & Bateman, T. C. Oriceps: Origami-inspired forceps. Smart Materials, Adaptive Structures and Intelligent Systems, 2013. American Society of Mechanical Engineers, V001T01A027.
[51] Kaufmann, J., Bhovad, P. & Li, S. 2022. Harnessing the multistability of kresling origami for reconfigurable articulation in soft robotic arms. Soft Robotics, 9, 212-223.
[52] Greenberg, H., Gong, M., Magleby, S. & Howell, L. 2011. Identifying links between origami and compliant mechanisms. Mechanical Sciences, 2, 217-225.